

COMMUNICATION



Cite this: *Energy Environ. Sci.*, 2021,

14, 890

Received 18th May 2020,

Accepted 12th January 2021

DOI: 10.1039/d0ee01578d

rsc.li/ees

Due to its high theoretical energy density and relative abundance of active materials, the magnesium–sulfur battery has attracted research attention in recent years. A closely related system, the lithium–sulfur battery, can suffer from serious self-discharge behavior. Until now, the self-discharge of Mg–S has been rarely addressed. Herein, we demonstrate for a wide variety of Mg–S electrolytes and conditions that Mg–S batteries also suffer from serious self-discharge. For a common Mg–S electrolyte, we identify a multi-step self-discharge pathway. Covalent S₈ diffuses to the metal Mg anode and is converted to ionic Mg polysulfide in a non-faradaic reaction. Mg polysulfides in solution are found to be meta-stable, continuing to react and precipitate as solid magnesium polysulfide species during both storage and active use. Mg–S electrolytes from the early, middle, and state-of-the-art stages of the Mg–S literature are all found to enable the self-discharge. The self-discharge behavior is found to decrease first cycle discharge capacity by at least 32%, and in some cases up to 96%, indicating this is a phenomenon of the Mg–S chemistry that deserves focused attention.

Introduction

Since its initial demonstration, the magnesium–sulfur (Mg–S) battery has received intense research interest due to what it promises: high theoretical energy capacity (3459 mA h cm⁻³) and widespread material availability (Mg is 2.1 wt% of the Earth's crust).^{1,2} Compared to lithium–sulfur batteries, where Li makes up only 0.002 wt% in the Earth's crust, the Mg–S battery is an attractive technology for large-scale energy storage. As another advantage, early research suggested that Mg cells

Self-discharge of magnesium–sulfur batteries leads to active material loss and poor shelf life†

Hunter O. Ford,^a Emily S. Doyle,^a Peng He,^a William C. Boggess,^b Allen G. Oliver,^b Tianpin Wu,^c George E. Sterbinsky^c and Jennifer L. Schaefer   ^a

Broader context

To avoid the most catastrophic effects of climate change, transportation must become fully electrified, thereby breaking a significant pillar of our dependence on fossil fuels. To make this transition more economically feasible and therefore more likely to take place, a wide variety of next generation rechargeable battery chemistries are being explored. These new chemistries should be safe, energy dense, and consist of sustainable and abundant materials. One example of promising next generation chemistries is the magnesium–sulfur battery. Since the first demonstration of the Mg–S battery, progress in improving this technology has been inspired by the lithium–sulfur system, which has received significantly more attention. A well-known challenge for Li–S is the tendency to self-discharge. From a practical standpoint, the importance of battery shelf-life cannot be overstated. In this work, we demonstrate that unfortunately the Mg–S system also suffers from severe self-discharge. In screening a wide variety of Mg–S battery conditions and formulations, and finding that all were susceptible to self-discharge, we hope to bring attention to this serious problem facing Mg–S batteries.

were resistant to the formation of dendrites during metal deposition, thereby avoiding a serious failure mechanism plaguing Li metal cells.^{3,4} In recent years however, it has been found that certain cell conditions and electrolyte formulations do in fact enable dendritic Mg deposition.^{5–7} Uncovering and pursuing solutions to such roadblocks is necessary for the technology to advance.

Similarly, the work presented here identifies another challenge that has been so-far largely overlooked for Mg–S. This challenge is the issue of self-discharge, wherein the active material in the cell reacts when the cell is under static conditions, leading to a loss in capacity. For real-world use, cells should ideally retain capacity at any depth of charge/discharge. The challenge of self-discharge in metal–sulfur batteries is intrinsically related to the polysulfide-shuttle phenomenon. The shuttle process is well described in the literature for both Mg–S and Li–S, and is one of the major challenges to be overcome for practical use of these technologies, as it contributes to short life-cycle and fast capacity fade in metal–sulfur batteries.^{2,8–10} Unwanted migration of sulfur species is responsible for self-discharge under static conditions and for

^a Department of Chemical and Biomolecular Engineering, University of Notre Dame, Notre Dame, IN 46556, USA. E-mail: Jennifer.L.Schaefer.43@nd.edu

^b Department of Chemistry and Biochemistry, University of Notre Dame, Notre Dame, IN 46556, USA

^c X-ray Science Division, Advanced Photon Source, Argonne National Laboratory, Lemont, IL 60439, USA

† Electronic supplementary information (ESI) available: Substantial additional discussion can be found. See DOI: 10.1039/d0ee01578d

inefficient charging under dynamic conditions. Some key differences are that under the static condition, the sulfur transport is governed only by concentration gradient driven diffusion and the species in the electrolyte are not electrochemically generated. Under dynamic conditions there is the additional impact of electromigration on polysulfide transport, and the polysulfide speciation is governed by electrochemical and chemical processes. These differences aside, it is expected that approaches for disrupting the static condition self-discharge problem can be useful for overcoming the dynamic-condition challenge, and *vice versa*, in addition to improving shelf-life.

Systematic investigations of the self-discharge process in Li–S batteries are numerous, and reveal that self-discharge can exceed 70% of the cell capacity if left unchecked.^{11–18} Unfortunately, many of the methods by which the self-discharge is disrupted in Li–S cells, such as the use of LiNO₃ to form a protective solid electrolyte interface (SEI) on the anode, are not applicable to Mg–S cells. In other words, solutions for disrupting the metal–sulfur battery self-discharge must be tailored to each unique chemistry to be effective, underscoring the importance of investigating the self-discharge of Mg–S. Remarkably, reports in the literature of the Mg–S static self-discharge are scarce, especially considering how much self-discharge has been studied in Li–S systems.

With the use of Raman spectroscopy, Vinayan and colleagues identified the formation of ionic S₈²⁻ under static conditions in Mg–S cells that employed a magnesium tetrakis(hexafluoroisopropoxy) borate (Mg[B(hfip)₄]₂) in 1,2-dimethoxyethane (DME) electrolyte. When the cells were assembled and held at their open circuit potential (OCP), the potential decreased over time and the anode impedance increased dramatically. The increase in impedance was attributed in part to the reaction between the anode and S₈²⁻, which resulted in the formation of a passivation layer.¹⁹ The authors suggested that S₈ was being converted to S₈²⁻ due to an interaction between S₈ and the ions in the electrolyte.

During an extensive electrochemical impedance spectroscopy (EIS) investigation on Mg–S cells using the same electrolyte, Häcker and colleagues also discovered a large increase in the charge transfer resistance associated with the Mg anode when a full cell was assembled and held under static conditions for 50 h. The increase in resistance was attributed in part to the diffusion of solubilized S₈ to the Mg anode where it underwent reduction.²⁰ Further, at elevated temperatures it was observed that the non-faradaic reduction of S₈ under static conditions was enhanced. This result is attributed to the increased solubility of S₈ and ionic polysulfides in the electrolyte at elevated temperatures, indicating that solubilized S₈ reacts directly with Mg metal to initiate self-discharge.

Very recently, the work by Häcker *et al.* on Mg–S self-discharge was expanded with computational methods, concluding that the self-discharge in Mg–S is faster than in Li–S, further indicating this is a serious challenge the Mg–S chemistry faces.²¹

To the best of our knowledge, these reports are the only investigations that deal in any capacity with the self-discharge of Mg–S batteries. In an effort to assess a road-block that has been largely ignored, we directly investigate the self-discharge

tendency of Mg–S batteries using a diverse set of electrolytes, and our findings are a wake-up call: every electrolyte investigated allows for self-discharge.

When Mg–S cells are held at OCP, whether they are partially discharged or fully charged, covalent S₈ is spontaneously converted to polysulfides through a non-faradaic reaction process. In some cases, the self-discharge is quite severe. What's more, unlike lithium polysulfides, magnesium polysulfides are found to be inherently unstable in solution, leading to the precipitation of active material. The precipitation effect is not limited to the static condition, as it is also found to be relevant at the timescales of active cell discharge. Uncontrolled precipitation of active material can result in permanent capacity loss if the material is inaccessible electronically or ionically, further contributing to the quick capacity fading woes of the Mg–S chemistry. Finally, the seriousness of the self-discharge is evaluated. Cells that self-discharge at OCP for 168 h see at least a 32% reduction in 1st cycle deliverable capacity. In some cases, depending on the electrolyte, the capacity reduction as a result of self-discharge exceeds 90%.

Given the wide variety of electrolyte chemistries explored and that self-discharge is observed in every case, it is clear that this is a phenomenon of Mg–S cells that should be addressed directly. As a first step in overcoming this problem, we have identified the initial reaction in the self-discharge pathway. The self-discharge begins when covalent S₈ dissolves in the electrolyte, diffuses to the metal Mg anode, and becomes reduced. For Mg–S compatible electrolytes, the spontaneous conversion of S₈ to an ionic form due to interaction with the electrolyte alone appears negligible; the presence of magnesium metal is required. Strategies that prevent contact of all sulfur species, S₈ and polysulfides, with the magnesium anode should be explored to help prevent self-discharge initiation. Stabilization of intermediate polysulfide species should be pursued to prevent active material loss *via* uncontrolled precipitation.

Results and discussion

Probing the self-discharge of a 0.25 M MgTFSI₂ + 0.5 M MgCl₂ + DME electrolyte

Since the first demonstration of reversible sulfur redox chemistry obtained with magnesium bis(trifluoromethanesulfonimide) (MgTFSI₂) + magnesium chloride (MgCl₂) based electrolytes, numerous works have made use of this chemistry for Mg–S investigations.^{8,22–27} Owing to the commercial availability and relative ease of preparation of this electrolyte, it has seen widespread use in various forms, *i.e.* in different ethereal solvents, salt concentrations, salt molar ratios, *etc.* The particular formulation of 0.25 M MgTFSI₂ + 0.5 M MgCl₂ in 1,2-dimethoxyethane (DME) originally reported by Gao and colleagues was selected as the initial electrolyte to be studied for self-discharge.²² With this electrolyte, the cell configuration used in this study, and a rate of 0.1C with respect to sulfur, the average 1st discharge capacity of Mg–S cells was found to be 396 ± 27 mA h g⁻¹ based on 13 cells discharged from OCP to 0.5 V (Fig. S17, ESI†). The SOC values throughout the rest of manuscript are in reference to this value.

Due to well-known issues with reversibility, which in addition vary greatly for different Mg–S electrolytes, this study is concerned with the self-discharge impact on pristine cells. By this approach, the effects of self-discharge are highlighted and not conflated with other challenges facing the Mg–S chemistry.

A series of cells were assembled using the 0.25 M MgTFSI₂ + 0.5 M MgCl₂ in DME electrolyte and were discharged to roughly half the average 1st discharge capacity, 200 mA h g⁻¹. After discharging to 200 mA h g⁻¹, the cells were allowed to age for different periods of time. Analogously, identical cells were assembled and held at OCP for the same amount of total time as the aged discharged cells. After the appropriate amount of time, the cells were opened, the components were extracted with tetrahydrofuran (THF), and the resulting solutions were analyzed *via* ultraviolet-visible spectroscopy (UV/VIS) to detect the presence of polysulfides. Additional experimental details are in the supplementary information. The THF extraction procedure was used so there would be a large enough sample volume to analyze, and because both S₈ and many ionic polysulfide species have sufficient solubility in THF. Solutions of S₈ in THF are clear and colorless with absorbance in the UV region, whereas polysulfides of many flavors have absorbance signatures in the UV and near UV regions, making the detection of both neutral and ionic sulfur with UV/VIS spectroscopy straightforward.^{23,28–33}

Fig. 1 shows the background subtracted absorbance spectra for the 200 mA h g⁻¹ discharged cells and the cells held at OCP. The background subtraction (described in detail in the ESI†) is such that any absorbance from solvent and salts is removed; only newly formed species in the electrolyte remain in the

spectra after subtraction. The 200 mA h g⁻¹ discharged sample analyzed immediately after discharging shows absorbance bands consistent with magnesium polysulfides. The spectrum bears qualitative resemblance to UV spectra collected on a similar system.³³ From the literature, the peak around 380 cm⁻¹ is likely S₄²⁻.^{32,33} While there remains some discrepancy in the literature about describing the characteristic absorbance wavelengths of other polysulfide species, attempts to identify the speciation in this case are moot anyways. The polysulfide speciation observed is likely not representative of the speciation within the cell, as the change in solvent environment and concentration occurring during sample preparation causes a change in polysulfide speciation.^{31,32}

The important point to consider is not the polysulfide speciation, but the total absorbance, as the area under the curve is assumed to be related to the polysulfide concentration. From the inset in Fig. 1 it is clear that as a 200 mA h g⁻¹ discharged cell ages, the concentration of polysulfide in the cell changes. The concentration increases, peaks, and then decreases. The increase in concentration is indicative of continued non-faradaic discharge, where S₈ that has not been electrochemically reacted is being converted to UV/VIS active polysulfides, *i.e.* self-discharge. The eventual decline in total absorbance hints at the instability of the formed polysulfides and continued chemical reaction.

Remarkably, an undischarged cell held at OCP for the same total time as the 24 h aged 200 mA h g⁻¹ discharged cell shows almost the same total absorbance and a nearly identical absorption spectrum as the electrochemically discharged cell. Under a static condition, a severe non-faradaic self-discharge

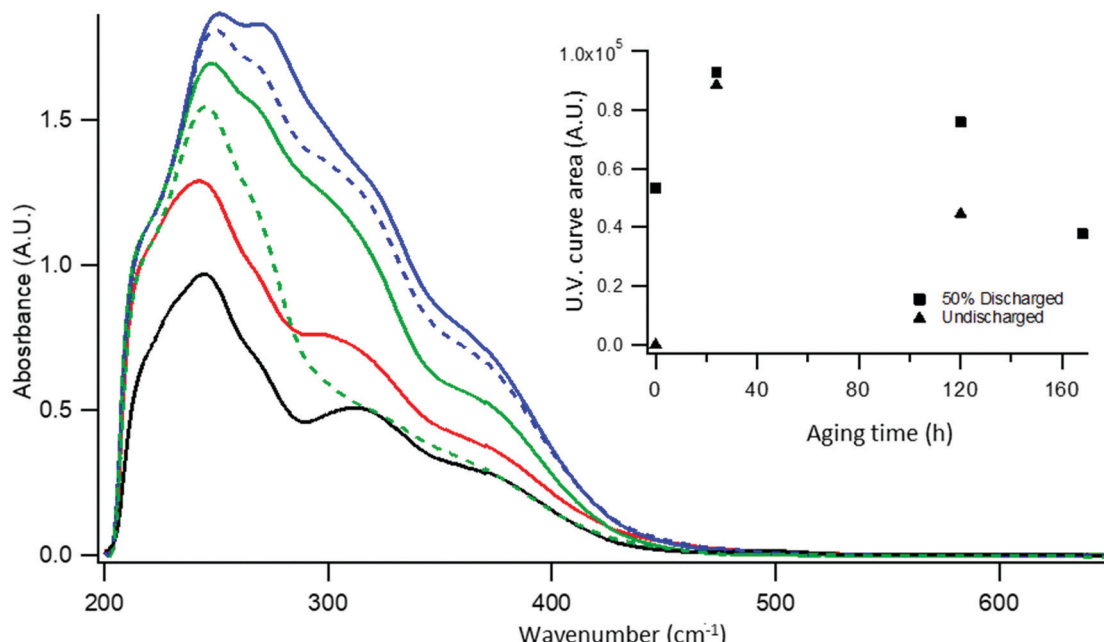


Fig. 1 Background subtracted UV/VIS absorbance spectra for extracted solutions from Mg–S cells using the 0.25 M MgTFSI₂ + 0.5 M MgCl₂ DME electrolyte. — 200 mA h g⁻¹ discharged cell aged 0 h. — 200 mA h g⁻¹ discharged cell aged 24 h. — 200 mA h g⁻¹ discharged cell aged 120 h. — 200 mA h g⁻¹ discharged cell aged 168 h. - - - Undischarged cell aged 24 h. - - - Undischarged cell aged 120 h. Inset shows total area under the spectra curves.

process is apparently active for this electrolyte, wherein a substantial amount of covalent sulfur is converted into UV/VIS active polysulfide species. The cells held at OCP follow a similar trend as those that are partially discharged, in that after a certain amount of time spent aging the polysulfide concentration starts to decrease.

These results demonstrate a severe static condition self-discharge problem for cells at various SOC. Further, the process appears to be multi-staged. During the early stages, covalent sulfur is converted to UV/VIS active polysulfides, increasing the polysulfide concentration. These polysulfide intermediates appear meta-stable, converting further to other species that are not active in UV/VIS (or perhaps insoluble in solution), indicated by the decrease in total absorbance over time. At later stages, this process results in the polysulfide concentration in solution decreasing.

In the process of opening the coin cells for the UV/VIS sample preparation, yellow-orange deposits visible to the naked eye were noticed on the separators and cathodes of the longer aged cells. These deposits are not soluble in pure THF or DME. The deposits were analyzed with a battery of techniques to understand their chemical composition, and are identified as solid magnesium polysulfides (Mg_xS_y).

Fig. 2A shows a photo of a separator recovered from a cell that was discharged to 200 mA h g^{-1} and aged for 168 h. Fig. 2B shows accompanying scanning electron microscopy with energy-dispersive X-ray spectroscopy (SEM-EDX) results of the large deposit for selected elements. The deposits found on the separator and on the cathode (Fig. 2 and Fig. S3–S5, ESI[†]) are chemically distinct from deposits of the electrolyte salts (Fig. S6, ESI[†]) in that the electrolyte deposits contain large amounts of Cl, F, and N, whereas the deposit in Fig. 2 and Fig. S3–S5 (ESI[†]) do not. Consisting predominantly of magnesium, sulfur, and oxygen (samples are briefly exposed to air when transferred into the SEM), the deposits are believed to be solid magnesium (poly)sulfides (Mg_xS_y).

It has been shown that in addition to the solid discharge products of MgS and MgS_2 , Mg –S cells can produce other solid products (chemically and electrochemically) such as Mg_3S_8 .³⁴ Using the same technique that was used previously to observe Mg_3S_8 , synchrotron X-ray absorption spectroscopy (XAS), the S K-edge of the deposits shown in Fig. 2A as well as that of covalent S_8 is interrogated, with the spectra shown in Fig. 2C. The deposit contains a pre-edge feature at 2469.9 eV, which is generally observed for ionic polysulfides.^{34,35} The feature is a result of the localization of the negative charge of the polysulfide anion on the terminal S atoms in the polysulfide chain. The presence of this feature indicates this sample is a solid magnesium polysulfide, as there are only Mg cations in this system. Unlike the literature spectra for Mg_3S_8 , the main edge feature of the Mg_xS_y deposit in this study is at 2471.8 eV, indicating the environment of sulfur atoms in this sample is closer to MgS_8 than Mg_3S_8 .³⁴ Analysis of the extended X-ray absorption fine structure (EXAFS) for the Mg_xS_y solid (Fig. S12, ESI[†]) shows a peak at 1.62 Å, which is less than that of S_8 (1.72 Å), less than MgS_8 within an *N*-methyl imidazolium coordination shell (1.67 Å), but

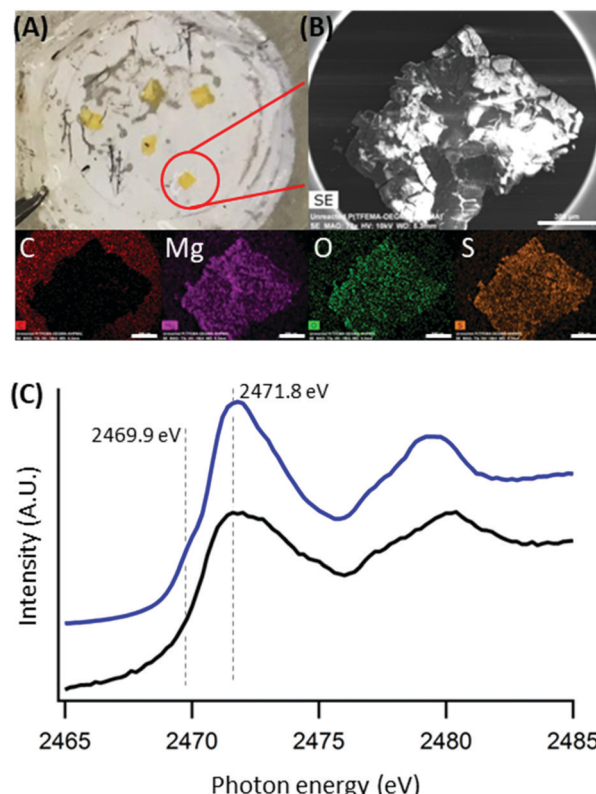


Fig. 2 (A) Photo of separator recovered from 200 mA h g^{-1} discharged cell, 168 h aged. (B) SEM image of highlighted deposit with accompanying EDX. All scale bars are 300 μm . (C) S K-edge XAS spectra for — Mg_3S_8 solid and for — elemental sulfur.

greater than that of Mg_3S_8 (1.30 Å).³⁴ As the sulfur atoms are more tightly coordinated than MgS_8 and looser than Mg_3S_8 , but the main K-edge feature is still at 2471.8 eV, the Mg_xS_y solid has a likely chemical composition of MgS_{6-8} .

In addition to SEM-EDX and XAS, this solid precipitate is probed with a host of other analytical techniques including an ultra performance liquid chromatography-mass spectroscopy (UPLC-MS) method, which is discussed in detail in the following section, powder X-ray diffraction (PXRD), and nuclear magnetic resonance (NMR) spectroscopy. The details of these results are discussed in the supporting information under the “Further Mg_xS_y Solid Analysis” section with Fig. S14–S16 (ESI[†]). The combination of these techniques allows for the definitive identification of this material as a solid magnesium polysulfide of likely formula MgS_{6-8} that is amorphous in nature and contained within a DME solvent shell.

Regardless of the exact chemistry, the presence of solid precipitates that contain large amounts of Mg and S that are chemically distinct from the electrolyte salts is further evidence of the proposed multi-stage self-discharge pathway. Magnesium polysulfides formed *via* both electrochemical and non-faradaic processes spontaneously precipitate from solution all across the cell. These deposits are formed in every single cell of this composition that is aged, being observed in dozens of cells, meaning this is a very reproducible and serious problem.

Spatially uncontrolled precipitation of active material has serious ramifications for Mg–S reversibility, and so this precipitation process was studied with an additional technique.

A UPLC-MS analysis capable of quantifying total ionic sulfur was applied to the Mg–S system.³⁶ This technique uses a derivatizing agent, 4-(dimethylamino)benzoyl chloride, to functionalize magnesium (poly)sulfides and yield a stable and quantifiable compound. According to Scheme S1, ionic magnesium (poly)sulfides are converted to difunctionalized neutral organic sulfides, D–S_x–D, where D represents the derivatizing agent. The resulting compounds are easily separable by molecular weight using UPLC and facilely ionized with the addition of a proton to one of the dimethylamino groups for MS detection and quantification.

Similar to the UV/VIS experiment, Mg–S cells were discharged to different SOC and rested for different amounts of time. The cathodes and separators from the cells were harvested and rinsed with DME to remove soluble polysulfides, leaving behind only the insoluble (poly)sulfide solids for derivatization and quantification. In the supplementary information (Fig. S33, ESI[†]), we demonstrate that the derivatizing agent easily reacts with insoluble ionic (poly)sulfide solids, allowing for accurate quantification of solid ionic sulfur. Further, the derivatizing agent has a negligible reaction with covalent sulfur, meaning any unreacted S₈ does not appear in the total sulfur count (Fig. S34, ESI[†]).

Fig. 3 shows the quantified solid sulfur observed for cells discharged to 200 mA h g⁻¹, 300 mA h g⁻¹, and 0.5 V (396 mA h g⁻¹ average). The immediately analyzed 200 mA h g⁻¹ discharged cells show a small amount of sulfur (near the technique detection limit), indicating that by 200 mA h g⁻¹ only a small amount of the active material has been reduced to a solid form,

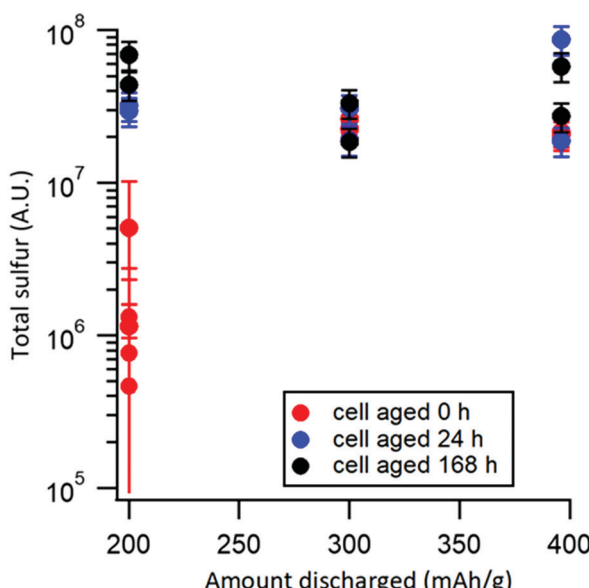


Fig. 3 Total solid ionic sulfur in separator and cathode detected by UPLC-mass spectroscopy method for cells discharged to various SOC and aged for various lengths of time prior to derivatization reaction.

electrochemically or chemically. Due to the proximity to detection limit, there were more data points taken for this set of samples. Cells that are discharged to 200 mA h g⁻¹ and aged for 24 h contain more solid ionic sulfur species than their immediately analyzed counterparts, by almost an order of magnitude. After 168 h of aging, even more sulfur is detected. The increase in detected ionic sulfur can only take place if additional solid (poly)sulfide species are present on the cathode and separator. In as little as 24 h, evidently a significant amount of solubilized polysulfides precipitate from solution.

The 300 mA h g⁻¹ and fully discharged (to 0.5 V, average 396 mA h g⁻¹) cells do not show a meaningful change in solid ionic sulfur content with aging, implying that by 300 mA h g⁻¹ of discharge the meta-stable species that chemically precipitate upon aging have been precipitated as ionic (poly)sulfides. Additionally, there must be little S₈ remaining in the cell, otherwise the initial stage of self-discharge would produce the meta-stable species that eventually precipitate. An experiment where the separator material is varied (Fig. S26 and S27, ESI[†]) reveals that the precipitation observed as the cell is discharged from 200 mA h g⁻¹ to 300 mA h g⁻¹ is a mixture of electrochemically and chemically driven precipitation, but mostly chemical precipitation. Even at the timescales of active discharge, the chemical precipitation of polysulfides, resulting in a permanent loss of active material, is highly relevant and poses a significant challenge to capacity retention.

From 300 mA h g⁻¹ to fully discharged, no change in the amount of solid ionic (poly)sulfides is observed. This result is explained by understanding the last stages of the Mg–S reduction are solid state reactions, and that this mass spectrometry technique cannot distinguish between different ionic (poly)sulfide species. It is possible that by 300 mA h g⁻¹ the electrochemically accessible active material is mostly in the Mg₃S₈ state (in agreement with Xu *et al.*)³⁴ and this is being converted to species such as Mg₂S and MgS as the cell approaches fully discharged. As far as this mass spectrometry technique is concerned, Mg₃S₈ and 8MgS will give the same quantitative result for total ionic sulfur.

In summary, the 0.25 M MgTFSI₂ + 0.5 M MgCl₂ in DME electrolyte suffers a severe self-discharge problem. The self-discharge occurs when the cell is at a full state of charge, or is partially discharged, and is evidenced by the non-faradaic production of polysulfides. The self-discharge appears to be a multistep process. First, covalent S₈ dissolves in the electrolyte, diffuses to the Mg anode, and then reacts to form magnesium polysulfides. The spontaneous production of polysulfides under static conditions is observed with the use of UV/VIS spectroscopy and additionally confirmed using the UPLC-MS protocol (Fig. S35, ESI[†]). The decrease in polysulfide concentration in the UV/VIS with aging, the formation of visible MgS_{6–8} deposits in the cell, and increased solid ionic sulfur content with aging as detected with mass spectrometry all point to a second stage in the self-discharge process: continued reaction of metastable polysulfides resulting in their eventual precipitation. The large-scale precipitation of active material occurs during active discharge in addition to static storage. The degree to which

active material is lost due to uncontrolled precipitation appears high, which could make for low sulfur utilization in subsequent cycles. In brief, the shelf-life of an Mg–S battery employing this electrolyte would be impractically short.

Self-discharge tendency with other Mg–S electrolytes

To evaluate how widespread the self-discharge problem is, a series of other Mg–S relevant electrolytes are evaluated and shown in Fig. 4. Three other electrolytes compatible with Mg–S chemistry as well as solutions of chemically synthesized magnesium polysulfides are analyzed using the established UV/VIS approach. The magnesium polysulfides are synthesized according to the literature from magnesium powder and sulfur powder in a solution of 0.25 M MgTFSI₂ + 0.5 M MgCl₂ in DME, with full details in the experimental section.²² The fact that this synthesis is possible is further direct confirmation of S₈ conversion to ionic polysulfides through a direct chemical reaction with Mg metal. Note, generally methods that are used to synthesize lithium polysulfides are not successful for the synthesis of magnesium polysulfides, especially in ethers. The magnesium polysulfide synthesis used here requires the presence of magnesium salts to

be successful, indicating the importance of ionic species and a complicated reaction pathway involving the Mg metal surface, magnesium salts, and sulfur. Formation of ionic polysulfides *via* this synthetic method was validated with the MS technique (Fig. S36, ESI[†]).

The other electrolytes studied are a concentrated form of the MgTFSI₂ + MgCl₂ in DME electrolyte (1 M MgTFSI₂, 2 M MgCl₂), an electrolyte based on magnesium bis(hexamethyldisilazide) (MgHMDS₂) and aluminum chloride (AlCl₃) in THF (0.35 M total Mg, 1:2 MgHMDS₂:AlCl₃), and an electrolyte consisting of 0.5 M magnesium fluorinated pinacolatoborate (MgFPB) in diglyme (DEG) that was first reported by Liu and colleagues in 2019.^{22,37,38} The salt and solvent structures, cyclic voltammetry induced Mg deposition/dissolution, and representative full cell discharges of each electrolyte are shown in the ESI,[†] in Fig. S1, S2, and S20, respectively.

The more concentrated form of the MgTFSI₂/MgCl₂ electrolyte is chosen because it has the same salts as the electrolyte investigated in the first part of this study, but has a decreased sulfur and polysulfide solubility owing to the high concentration of the magnesium salts.²² The MgHMDS₂/AlCl₃ electrolyte is chosen as

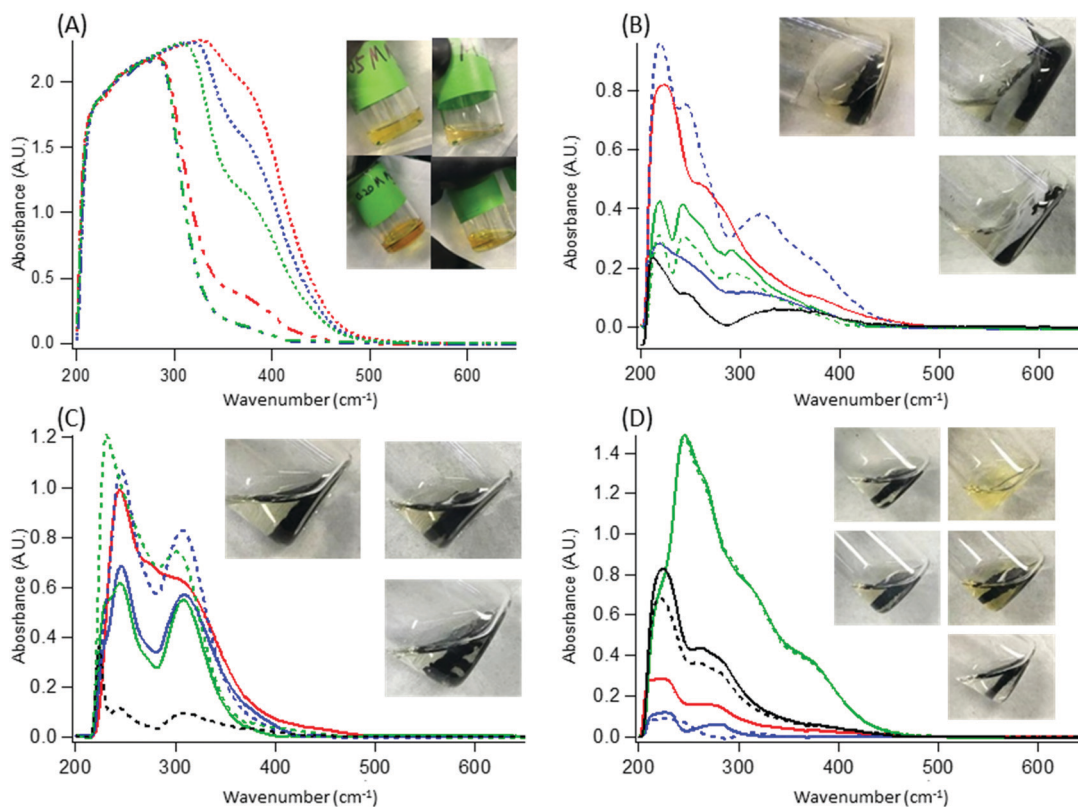


Fig. 4 UV/VIS spectra for (A) Synthesized magnesium polysulfides. 0.2 M sulfur aged 0 h. 0.2 M sulfur aged 24 h. 0.2 M sulfur aged 72 h. — 0.05 M sulfur aged 0 h. — 0.05 M sulfur aged 24 h. — 0.05 M sulfur aged 72 h. — 200 mA h g⁻¹ discharged cell aged 0 h. — 200 mA h g⁻¹ discharged cell aged 24 h. — 200 mA h g⁻¹ discharged cell aged 72 h. — 200 mA h g⁻¹ discharged cell aged 168 h. — Undischarged cell aged 24 h. — Undischarged cell aged 72 h. — Undischarged cell aged 168 h. (B) 1 M MgTFSI₂ + 2 M MgCl₂ in DME. — 200 mA h g⁻¹ discharged cell aged 0 h. — 200 mA h g⁻¹ discharged cell aged 24 h. — 200 mA h g⁻¹ discharged cell aged 72 h. — Undischarged cell aged 24 h. — Undischarged cell aged 72 h. (C) 0.35 M Mg – 1:2 MgHMDS₂:AlCl₃. (D) 0.5 M MgFPB in DEG. Insets are photos of selected solutions analyzed by UV/VIS; black material in the photos are the extracted cathodes. Inset (A) top left = 0.05 M solution as prepared. Top right = 0.05 M solution 72 h aged. Bottom left = 0.2 M solution as prepared. Bottom right = 0.2 M solution 72 h aged. Inset (B/C) top left = 200 mA h g⁻¹ discharged immediate analysis. Top right = undischarged 24 h aged. Bottom = reference solution for background subtraction. Inset (D) top left = 200 mA h g⁻¹ discharge 24 h aged. Top right = 200 mA h g⁻¹ discharge 72 h aged. Middle left = undischarged 24 h aged. Middle right = undischarged 72 h aged. Bottom = reference solution for background subtraction.

it is one of the earliest Mg–S compatible electrolytes, with THF selected as the solvent owing to its enhanced Mg deposition/dissolution reversibility relative to other ethers.^{37,39} The MgFPB electrolyte represents a current generation chloride-free and high coulombic efficiency electrolyte, which owing to its chemical similarity to the Mg[B(hfip)₄]₄ based electrolyte and non-nucleophilic nature, is expected to be compatible with sulfur.^{19,20,38}

Samples from each electrolyte are prepared with a similar procedure to the previously discussed UV/VIS experiment. An aliquot from the synthesized magnesium polysulfide solutions, of which there are two varying concentrations, is extracted and likewise analyzed by UV/VIS. Fig. 4A–D contains the results for each respective solution/electrolyte, with the inset photographs showing the analyzed solution (black material is cathode undergoing extraction). Compared to Fig. 4B, C, and D, Fig. 4A has a different general absorbance pattern due to the background solution used for that set of samples. Fig. 4A shows covalent S₈ in the spectrum in addition to the polysulfides. See Fig. S23 (ESI[†]) for further discussion and Fig. S24 and S25 (ESI[†]) for UV/VIS spectra of magnesium polysulfides chemically synthesized in the MgHMDS₂/AlCl₃ and MgFPB electrolytes.

Although the detailed trends for each electrolyte are different, two major trends are observed in every case. Firstly, all electrolytes show spontaneous formation of polysulfides and therefore suffer from self-discharge. The cells held at OCP all produce UV active species that resemble the absorbance spectra of the immediately analyzed, electrochemically discharged cells. The self-discharge process is strong enough that a visible color change to characteristic polysulfide yellow is observable with the naked eye in many cases. Secondly, the polysulfides in each solution are metastable, changing in concentration and specific absorbance pattern depending on the age of the cell. This suggests the second portion of the self-discharge process, continued reaction of meta-stable polysulfides, is also active in these electrolytes to varying extents. Regarding Fig. 4A, the decrease in absorbance accompanied by formation of precipitate in the synthesized polysulfide solution suggests the instability of the polysulfides is in part inherent, and not totally reliant on the presence of magnesium metal for continued reaction.

Of all the responses, perhaps the most interesting is observed in Fig. 4D with the MgFPB electrolyte, where initially the formation of polysulfides is quite suppressed in both the discharged cells and those held at OCP. At some point between 24 and 72 h of aging, a dramatic increase in polysulfide concentration occurs. The absorbance patterns and total concentration of the 72 h aged MgFPB samples are very similar to that of the 120 h aged, 200 mA h g⁻¹ discharged 0.25 M MgTFSI₂ + 0.5 M MgCl₂ electrolyte in Fig. 1. Between 72 h and 168 h, the polysulfide concentration drops again in the MgFPB electrolyte, implying continued loss of active material for this system as well. This non-linear and dramatic change in the MgFPB solution holds particular importance for cycling this electrolyte, as the evolving cell chemistry would undoubtedly affect the cycling behavior. Depending on the conditions (*i.e.* cycling rate) the impacts of the changing solution chemistry could be varied and potentially misattributed to other processes

in the cell. The non-linear effect of aging on cells using this electrolyte deserves further attention to be fully understood.

The results of Fig. 4 suggest that the two stages in the self-discharge process (conversion of covalent sulfur to ionic polysulfides, precipitation of ionic sulfur) have different apparent kinetics, which may be controlled by the nature of the electrolyte. The solubility and diffusivity of covalent sulfur control the rate by which ionic polysulfides can be produced, *i.e.* in a low solubility/low diffusivity case, the production of polysulfides becomes mass-transport limited with respect to getting covalent sulfur to the Mg electrode. The solubility limit and stability of the polysulfides produced are dependent on the chemical environment, influenced by factors such as the salt concentration, solvent donor number, and the electrolyte salts, which is why the detailed trends vary across electrolytes.^{32,40,41}

In an effort to better understand the behavior observed in Fig. 4, the solubility of S₈ in each solvent and electrolyte was estimated (Table S3, ESI[†]), and EIS measurements as well as SEM/EDX analysis of the anodes and separators for each electrolyte in Fig. 4 were performed (Fig. S8–S11 and S22, ESI[†]). The results shown in Table S3 (ESI[†]) reiterate that S₈ solubility is only part of the picture in regards to self-discharge. For instance, the 0.25 M MgTFSI₂ + 0.5 M MgCl₂ in DME and the MgFPB in DEG electrolytes have similar S₈ solubility, but the former electrolyte develops polysulfides due to self-discharge much faster than the latter (24 h *vs.* 72 h). Additionally, even though the MgHMDS₂ + AlCl₃ in THF electrolyte has a high S₈ solubility, the total polysulfide concentration at its maximum is lower than that of the MgFPB in DEG and 0.25 M MgTFSI₂ + 0.5 M MgCl₂ in DME electrolytes, both of which have lower S₈ solubility. Clearly, the self-discharge is influenced heavily by reaction kinetics in addition to S₈ and polysulfide mass transport. This conclusion was recently reproduced independently of this work.²¹

SEM/EDX analysis of the separator and anode after cell aging provides crucial insight to the process governing the precipitation of active material. If the electrolyte has high polysulfide solubility, the active material precipitates across the entire cell, predominately where the electrolyte volume is stored (*i.e.* in the separator). If the polysulfide solubility is low, the active material precipitates on the surface of the Mg anode. Take for instance the result of Fig. 2. The 0.25 M TFSI₂ + 0.5 M MgCl₂ in DME electrolyte used to make that cell has a relatively high polysulfide solubility, and widespread precipitation of active material in the separator is observed.²² This precipitation is driven by the instability of the solubilized polysulfides. EDX analysis of the Mg anode in that case finds very little S on the surface that is not associated with S in the TFSI salt (Fig. S7, ESI[†]). Similarly, the THF based MgHMDS₂ + AlCl₃ electrolyte shows no S containing deposits on the Mg surface, but S rich deposits on the separator (Fig. S10 and S11, ESI[†]). In contrast, the low polysulfide solubility electrolytes like the 1 M MgTFSI₂ + 2 M MgCl₂ in DME²² and the early stage MgFPB in DEG show numerous large scale sulfur rich deposits on the Mg anode (Fig. S8 and S9, ESI[†]). These deposits are distinct from the electrolyte deposits, indicating they are from a reaction of the Mg anode with sulfur/polysulfides.

In cells with high polysulfide solubility limits, the self-discharge process results in S_8 converting to ionic polysulfides on the Mg anode surface. The newly formed magnesium polysulfide remains dissolved in the electrolyte, diffuses away from the anode, and any instability driven precipitation happens throughout the cell. In the case of low solubility electrolytes, the saturation limit for magnesium polysulfides in the electrolyte is quickly reached during self-discharge. After the saturation limit is reached, continued reaction of S_8 to ionic polysulfides that happens on the Mg surface results in immediate precipitation of the formed species on the Mg metal in large clusters.

Self-discharge impact on cell capacity

Having identified self-discharge behavior in a diverse set of electrolytes, the impact of self-discharge on the electrochemical performance of Mg–S cells is examined next and is found to be severe. Fully charged Mg–S cells using two different electrolytes are allowed to age at OCP for 168 h, during which the potential across the cell decreases from the initial OCP (Fig. S21, ESI[†]). As can be seen in Fig. 5, after aging the capacity delivered on the first cycle discharge is decreased significantly compared to pristine cells. After aging, the cells with either electrolyte require a period of activation wherein a massive overpotential for initiating the discharge redox chemistry must first be overcome. As observed in the literature and here *via* EIS (Fig. S22, ESI[†]), this high overpotential is likely due to increased impedance on the Mg anode as a result of the formation of passivation and/or absorption layers.^{19,20,24,33} Evidently, these layers become breached or displaced after a period of time and the potential stabilizes.

Even though they have similar levels of self-discharge according to the UV/VIS data, the massive capacity fade and decrease of discharge potential of the $MgTFSI_2 + MgCl_2$ electrolyte compared to the MgFPB hints at what may make for a better

electrolyte. Being a complex electrolyte, perhaps the presence of polysulfides in the $MgTFSI_2 + MgCl_2$ solution shifts the complex equilibria, resulting in fewer electrochemically active magnesium species. Additionally, the continued breakdown of chemically unstable $MgTFSI^+$ resulting in depletion of electrolyte salts over the aging period may be partly to blame for the poor performance.⁴²

Even though the MgFPB electrolyte loses capacity and suffers a high initial overpotential as a result of self-discharge, after activation the 168 h aged MgFPB discharge profile resembles that of the 0 h aged cell. These results suggest that the shelf-life of Mg–S can be enhanced by using simple magnesium salts that are not susceptible to changes in chemical equilibria, that have good stability on the electrode surface, and that stabilize polysulfide intermediates.

Conclusions

Self-discharge of Mg–S cells was observed in every instance for a set of diverse electrolytes. Further, this process decreased cell capacity by 32% and 96% for MgFPB and $MgTFSI_2 + MgCl_2$ based electrolytes, respectively, after a 168 h OCP hold period. It is proposed that S_8 in the cell undergoes non-faradaic reduction to ionic polysulfides at the Mg electrode surface, which then continue to chemically react and precipitate from solution. The location where the active material precipitates is dictated by the solution chemistry; high sulfur/polysulfide solubility leads to active material precipitating everywhere in the cell, whereas low solubility results in precipitation of active material on the Mg anode. The precipitation effect occurs at timescales relevant even to active discharge, making it a serious challenge to address. The apparent lack of any Mg–S electrolyte that prevents self-discharge is a clear call to researchers to continue electrolyte development and begin examining Mg–S self-discharge. With the work presented herein, we hope to offer the tools with which future electrolytes can be screened for self-discharge. Additionally, we believe our results prompt continued investigation in the following areas to address the self-discharge problem:

1. **Electrolyte development.** Electrolytes that limit (or eliminate) sulfur and polysulfide solubility should be investigated, thereby preventing contact of sulfur species with the anode. Sparingly soluble and solid-state electrolytes have been shown for Li–S systems to alter the redox pathways of the sulfur intermediates, in some cases avoiding reactive intermediates.^{40,43,44} In cases where polysulfide solubility is eliminated and the sulfur redox chemistry is restrained to solid-state reactions, Mg^{2+} transport and overall reaction kinetics will need to be addressed and improved. If polysulfide solubility cannot be eliminated, the polysulfides should be stabilized by electrolyte or cathode additives/components to prevent active material precipitation and loss.

2. **Engineered mass transport control.** Preventing contact of S_8 with the metal anode will prevent the first step of self-discharge. This may be accomplished with molecule selective membranes, an artificial Mg SEI, advanced cathode architectures, *etc.*

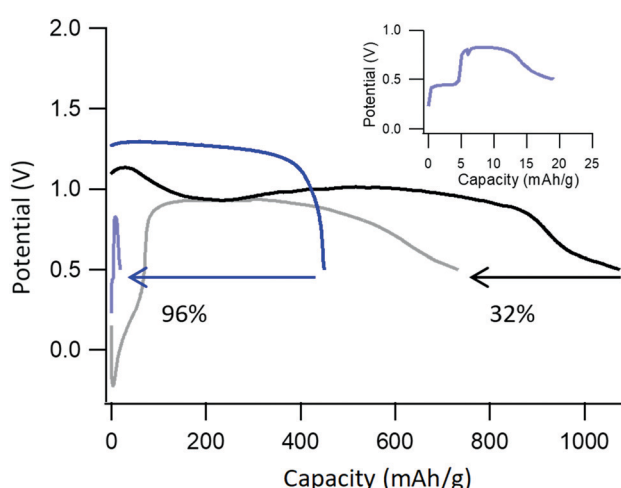


Fig. 5 1st cycle discharge potential/capacity traces for Mg–S cells at current rate of 0.1C. — 0 h aged 0.5 M MgFPB in DEG. — 168 h aged 0.5 M MgFPB in DEG. — 0 h aged 0.25 M $MgTFSI_2 + 0.5 M MgCl_2$ in DME. — 168 h aged 0.25 M $MgTFSI_2 + 0.5 M MgCl_2$ in DME. Inset shows the 168 h aged $MgTFSI_2/MgCl_2$ potential curve, enlarged for clarity.

3. Complete mechanistic, kinetic, and chemical description of the self-discharge process, especially understanding and disrupting the non-faradaic S₈-to-polysulfide reaction pathway. The importance of Mg surface species (MgCl₂, MgF₂), various ions such as the role of chloride, solvent, etc. must be understood. Fundamental results from this thrust will influence the direction of points 1 and 2.

Conflicts of interest

There are no conflicts to declare.

Acknowledgements

Funding for this work was received from the National Science Foundation *via* award number CBET-1706370 and from Amazon Catalyst at ECS, for which the authors are greatly appreciative. HOF gratefully acknowledges The Society of Schmitt Fellows, the Notre Dame CEST Predoctoral Fellowship, and the Patrick and Jana Eilers Fellowship for additional financial support. X-ray absorption spectroscopy measurements were carried out at beamline 9-BM of the Advanced Photon Source (APS). This research used resources of the APS, a U.S. Department of Energy (DOE) Office of Science User Facility operated for the DOE Office of Science by Argonne National Laboratory under Contract No. DE-AC02-06CH11357. The authors thank the Notre Dame Materials Characterization Facility, the Notre Dame Mass Spectroscopy and Proteomics Facility, the Notre Dame Molecular Structure Facility, and the Notre Dame Integrated Imaging Facility.

Notes and references

- 1 W. M. Haynes, *CRC Handbook of Chemistry and Physics*, 97th edn, 2016, pp. 14–17.
- 2 H. S. Kim, T. S. Arthur, G. D. Allred, J. Zajicek, J. G. Newman, A. E. Rodnyansky, A. G. Oliver, W. C. Boggess and J. Muldoon, *Nat. Commun.*, 2011, **2**, 427.
- 3 R. Mohtadi and F. Mizuno, *Beilstein J. Nanotechnol.*, 2014, **5**, 1291–1311.
- 4 J. Song, E. Sahadeo, M. Noked and S. B. Lee, *J. Phys. Chem. Lett.*, 2016, **7**, 1736–1749.
- 5 R. Davidson, A. Verma, D. Santos, F. Hao, C. Fincher, S. Xiang, J. Van Buskirk, K. Xie, M. Pharr, P. P. Mukherjee and S. Banerjee, *ACS Energy Lett.*, 2019, **4**, 375–376.
- 6 M. S. Ding, T. Diemant, R. J. Behm, S. Passerini and G. A. Giffin, *J. Electrochem. Soc.*, 2018, **165**, A1983–A1990.
- 7 R. Davidson, A. Verma, D. Santos, F. Hao, C. D. Fincher, D. Zhao, V. Attari, P. Schofield, J. Van Buskirk, A. Fraticelli-Cartagena, T. E. G. Alivio, R. Arroyave, K. Xie, M. Pharr, P. P. Mukherjee and S. Banerjee, *Mater. Horiz.*, 2020, **7**, 843–854.
- 8 P. Wang and M. R. Buchmeiser, *Adv. Funct. Mater.*, 2019, **29**, 1905248.
- 9 A. Manthiram, Y. Fu and Y. S. Su, *Acc. Chem. Res.*, 2013, **46**, 1125–1134.
- 10 Y. X. Yin, S. Xin, Y. G. Guo and L. J. Wan, *Angew. Chem., Int. Ed.*, 2013, **52**, 13186–13200.
- 11 J. Zhu, C. Chen, Y. Lu, J. Zang, M. Jiang, D. Kim and X. Zhang, *Carbon*, 2016, **101**, 272–280.
- 12 H. S. Ryu, H. J. Ahn, K. W. Kim, J. H. Ahn, K. K. Cho and T. H. Nam, *Electrochim. Acta*, 2006, **52**, 1563–1566.
- 13 M. L. Gordin, F. Dai, S. Chen, T. Xu, J. Song, D. Tang, N. Azimi, Z. Zhang and D. Wang, *ACS Appl. Mater. Interfaces*, 2014, **6**, 8006–8010.
- 14 M. Liu, Q. Li, X. Qin, G. Liang, W. Han, D. Zhou, Y. B. He, B. Li and F. Kang, *Small*, 2017, **13**, 1602539.
- 15 L. Wang, J. Liu, S. Yuan, Y. Wang and Y. Xia, *Energy Environ. Sci.*, 2016, **9**, 224–231.
- 16 H. S. Ryu, H. J. Ahn, K. W. Kim, J. H. Ahn, J. Y. Lee and E. J. Cairns, *J. Power Sources*, 2005, **140**, 365–369.
- 17 J. Q. Huang, T. Z. Zhuang, Q. Zhang, H. J. Peng, C. M. Chen and F. Wei, *ACS Nano*, 2015, **9**, 3002–3011.
- 18 W. T. Xu, H. J. Peng, J. Q. Huang, C. Z. Zhao, X. B. Cheng and Q. Zhang, *ChemSusChem*, 2015, **8**, 2892–2901.
- 19 B. P. Vinayan, H. Euchner, Z. Zhao-Karger, M. A. Cambaz, Z. Li, T. Diemant, R. J. Behm, A. Gross and M. Fichtner, *J. Mater. Chem. A*, 2019, **7**, 25490–25502.
- 20 J. Häcker, C. Danner, B. Sievert, I. Biswas, Z. Zhao-Karger, N. Wagner and K. A. Friedrich, *Electrochim. Acta*, 2020, **338**, 135787.
- 21 R. Richter, J. Häcker, Z. Zhao-Karger, T. Danner, N. Wagner, M. Fichtner, K. A. Friedrich and A. Latz, *ACS Appl. Energy Mater.*, 2020, **3**, 8457–8474.
- 22 T. Gao, S. Hou, F. Wang, Z. Ma, X. Li, K. Xu and C. Wang, *Angew. Chem., Int. Ed.*, 2017, **56**, 13526–13530.
- 23 H. O. Ford, L. C. Merrill, P. He, S. P. Upadhyay and J. L. Schaefer, *Macromolecules*, 2018, **51**, 8629–8636.
- 24 A. Robba, A. Vizintin, J. Bitenc, G. Mali, I. Arčon, M. Kavčič, M. Žitnik, K. Bučar, G. Aquilanti, C. Martineau-Corcos, A. Randon-Vitanova and R. Dominko, *Chem. Mater.*, 2017, **29**, 9555–9564.
- 25 Y. Bi, J. Luo, B. Hu, S. He, K. Nielson and T. L. Liu, *ECS Trans.*, 2017, **80**, 343–348.
- 26 P. He, H. O. Ford, L. C. Merrill and J. L. Schaefer, *ACS Appl. Energy Mater.*, 2019, **2**, 6800–6807.
- 27 T. Gao, X. Ji, S. Hou, X. Fan, X. Li, C. Yang, F. Han, F. Wang, J. Jiang, K. Xu and C. Wang, *Adv. Mater.*, 2018, **30**, 2–9.
- 28 M. U. M. Patel, R. Demir-Cakan, M. Morcrette, J. M. Tarascon, M. Gaberscek and R. Dominko, *ChemSusChem*, 2013, **6**, 1177–1181.
- 29 N. Xu, T. Qian, X. Liu, J. Liu, Y. Chen and C. Yan, *Nano Lett.*, 2017, **17**, 538–543.
- 30 Q. Zou and Y. C. Lu, *J. Phys. Chem. Lett.*, 2016, **7**, 1518–1525.
- 31 G. Bieker, J. Wellmann, M. Kolek, K. Jalkanen, M. Winter and P. Bieker, *Phys. Chem. Chem. Phys.*, 2017, **19**, 11152–11162.
- 32 G. Bieker, D. Diddens, M. Kolek, O. Borodin, M. Winter, P. Bieker and K. Jalkanen, *J. Phys. Chem. C*, 2018, **122**, 21770–21783.
- 33 M. Salama, R. Attias, B. Hirsch, R. Yemini, Y. Gofer, M. Noked and D. Aurbach, *ACS Appl. Mater. Interfaces*, 2018, **10**, 36910–36917.

34 Y. Xu, Y. Ye, S. Zhao, J. Feng, J. Li, H. Chen, A. Yang, F. Shi, L. Jia, Y. Wu, X. Yu, P. A. Glans-Suzuki, Y. Cui, J. Guo and Y. Zhang, *Nano Lett.*, 2019, **19**, 2928–2934.

35 T. A. Pascal, K. H. Wujcik, J. Velasco-Velez, C. Wu, A. A. Teran, M. Kapilashrami, J. Cabana, J. Guo, M. Salmeron, N. Balsara and D. Prendergast, *J. Phys. Chem. Lett.*, 2014, **5**, 1547–1551.

36 D. Qu, D. Zheng, D. Qu, X. Q. Yang, X. Yu and H. S. Lee, *Adv. Energy Mater.*, 2015, **5**, 1401888.

37 Z. Zhao-Karger, X. Zhao, O. Fuhr and M. Fichtner, *RSC Adv.*, 2013, **3**, 16330–16335.

38 J. Luo, Y. Bi, L. Zhang, X. Zhang and T. L. Liu, *Angew. Chem. Int. Ed.*, 2019, **58**, 6967–6971.

39 L. C. Merrill and J. L. Schaefer, *Langmuir*, 2017, **33**, 9426–9433.

40 C. W. Lee, Q. Pang, S. Ha, L. Cheng, S. D. Han, K. R. Zavadil, K. G. Gallagher, L. F. Nazar and M. Balasubramanian, *ACS Cent. Sci.*, 2017, **3**, 605–613.

41 A. Gupta, A. Bhargav and A. Manthiram, *Adv. Energy Mater.*, 2019, **9**, 1803096.

42 N. N. Rajput, X. Qu, N. Sa, A. K. Burrell and K. A. Persson, *J. Am. Chem. Soc.*, 2015, **137**, 3411–3420.

43 X. Yang, J. Luo and X. Sun, *Chem. Soc. Rev.*, 2020, **49**, 2140–2195.

44 E. Umeshbabu, B. Zheng and Y. Yang, *Electrochem. Energy Rev.*, 2019, **2**, 199–230.